applied optics

Extended shift-rotation method for absolute interferometric testing of a spherical surface with pixel-level spatial resolution

YU LIU, LIANG MIAO, WENLONG ZHANG, CHUNSHUI JIN, AND HAITAO ZHANG*

State Key Laboratory of Applied Optics, Changchun Institute of Optics, Fine Mechanics and Physics, Chinese Academy of Sciences, Changchun 130033, China

*Corresponding author: zhanght@sklao.ac.cn

Received 14 March 2017; revised 10 May 2017; accepted 10 May 2017; posted 11 May 2017 (Doc. ID 290379); published 1 June 2017

An improved shift-rotation method for the absolute testing of spherical surfaces is developed to obtain pixel-level spatial resolution and a low noise propagation ratio. The absolute testing process includes multiple rotational tests and two lateral shifting tests with large shifts. A wavefront reconstruction algorithm based on subaperture division and least squares fitting is proposed to reconstruct the surface figure of the test optics. Numerical simulation results show that the method reveals high-frequency figures missed in the traditional Zernike-based shift-rotation method. The algorithm error is lower than 0.4%, and the noise propagation ratio can be reduced by 70% using large shifts. The absolute testing of spherical optics is carried out to verify this method. One spherical surface was tested with the presented absolute testing method and the method using a point diffraction interferometer. The difference of the measurement results based on the two methods showed that the testing uncertainty reached 0.19 nm root mean square (RMS), which indicated that the presented method has potential subnanometer testing uncertainty.

OCIS codes: (120.3180) Interferometry; (120.3940) Metrology; (120.6650) Surface measurements, figure.

https://doi.org/10.1364/AO.56.004886

1. INTRODUCTION

The surface figures of spherical surfaces are usually tested using commercial Fizeau interferometers, and the testing accuracy depends on the system error of the interferometers. The main system error is the reference surface of the transmission sphere, which is usually no better than $\lambda/40$ PV (around 2 nm root mean square (RMS), $\lambda = 633$ nm). Many absolute testing methods have been developed to achieve subnanometer testing accuracy. The lateral shearing method [1–3] and shift-rotation method [4–7] are widely used absolute testing methods for spherical surfaces. Both methods require testing data at multiple positions to separate the surface figure of the test optics from the system error of the interferometer.

The lateral shearing method requires testing results at one original position and multiple lateral shifting positions. The entire surface figure of the test optics can be reconstructed from finite difference equations comprising all the testing results. The typical wavefront reconstruction algorithm is a pixel-based least squares fitting, which can reveal the surface figure with pixel-level spatial resolution. However, the noise propagation ratio is high because the shifting distance of this method is usually limited to one pixel to avoid a singular solution [3]. In addition, the tilt change of the test optics during lateral shifting will cause errors in the Zernike quadratic terms, such as power and astigmatism [8,9]. Therefore, obtaining an accurate astigmatism aberration of the surface figure is difficult. Power aberration is the concept of defocus, which is an alignment term, and depends on the distance between the reference surface and the testing optics [10]; therefore, power aberration is of little concern in the testing of spherical surfaces.

The shift-rotation method needs testing results at N rotational positions and one lateral shifting position. The N rotational position samples of the shift-rotation method are equidistant. Most of the rotationally asymmetric surface figures of the test optics will be obtained accurately from the rotational results [7,11]. Rotationally symmetric terms and $kN\theta$ terms of the surface figure are reconstructed from a series of finite difference equations comprising the lateral shifting results [11]. The wavefront reconstruction algorithm for the difference equations is based on the Zernike polynomial fitting, which can only characterize low-frequency figures [5,8]. As a result, high-frequency rotational terms and $kN\theta$ terms (k is a positive integer, N is the total number of rotational measurements, $\theta = 2\pi/N$) are missed in the traditional Zernike-based shift-rotation method [5].

However, high-frequency figure information is needed in some circumstances. One example is the figure error testing of the null lens for aspheric mirrors used in Extreme Ultraviolet Lithography, in which the figure errors higher than 1 cycles/mm are required [12]. For this case, high-frequency figure information cannot be obtained via the traditional Zernike-based shift-rotation method. Thus, a new absolute testing technique needs to be developed to acquire high-frequency figure information.

In this paper, an extended shift-rotation method for absolute interferometric testing with pixel-level spatial resolution is presented. The extended shift-rotation method combines the advantages of the traditional shift-rotation and the lateral shearing methods, so that the surface figure of spherical surfaces can be obtained absolutely with pixel-level spatial resolution and a low noise propagation ratio. When the tilt of the test optics is controlled by other ways [9], this method can also be used for absolute testing of plane surfaces.

In the second section, the testing procedure and principle of the extended shift-rotation method is introduced. Then, the wavefront reconstruction algorithm applicable for large shifts is proposed to improve the noise propagation ratio and avoid a singular solution. In the third section, numerical simulation and absolute testing experiments are carried out to verify the characteristics of the presented method and the wavefront reconstruction algorithm. In the fourth section, the absolute testing of spherical optics is carried out to verify this method. One spherical surface was tested with the presented absolute testing method and the method using a point diffraction interferometer (PDI). The difference between the two methods showed that the testing uncertainty of the absolute testing is 0.19 nm RMS. The results indicated that the presented method has potential subnanometer testing uncertainty with high spatial frequency.

2. ABSOLUTE TESTING PROCEDURE AND WAVEFRONT RECONSTRUCTION ALGORITHM

The presented method extends the traditional shift-rotation and the lateral shearing methods. The testing procedure includes N equispaced rotational tests and two orthogonal lateral shifting tests. Let $W(x,y)$ be the surface figure of the test optics, $V(x,y)$ be the system error of the interferometer, and $T(x,y)$ be the test result. Here, (x,y) is the coordinate defined on the charge-coupled device (CCD) sensor of the interferometer. The above three terms satisfy

$$T(x,y) = W(x,y) + V(x,y). \tag{1}$$

First, N equispaced rotational tests are carried out. The test result at each rotational angle is expressed as

$$T_\phi(x,y) = W_\phi(x,y) + V(x,y),$$
$$(\phi = 0, 2\pi/N, 4\pi/N, \ldots, 2\pi(N-1)/N). \tag{2}$$

The surface figure can be separated into two components, namely, rotationally asymmetric terms $W^{\mathrm{asym}}(x,y)$ and rotationally symmetric terms $W^{\mathrm{sym}}(x,y)$. By averaging the test results at all rotational angles, we can obtain the following:

$$\bar{T}(x,y) = \frac{1}{N}\sum_{i=1}^{N} T_{\phi_i}(x,y)$$
$$= W^{\mathrm{sym}}(x,y) + W^{kN\theta}(x,y) + V(x,y), \tag{3}$$

where $W^{kN\theta}(x,y)$ are $kN\theta$ terms, which are $2\pi/kN$ rotationally symmetric radians. The $kN\theta$ terms belong to rotationally asymmetric terms and can be expressed by Zernike polynomials [10],

$$W^{kN\theta}(x,y) = \sqrt{2(n+1)}\begin{Bmatrix} \cos kN\theta \\ \sin kN\theta \end{Bmatrix} R_n^{kN}(\rho),$$
$$\times \begin{pmatrix} k = 1, 2, 3, \ldots \\ n = kN, kN+2, kN+4, \ldots \\ \rho = \sqrt{x^2+y^2} \end{pmatrix}. \tag{4}$$

Subtracting Eq. (3) from Eq. (2) cancels the system error and leads to the following equation for the test optics:

$$T_\phi(x,y) - \bar{T}(x,y) = W_\phi^{\mathrm{asym}}(x,y) - W^{kN\theta}(x,y), \tag{5}$$

where $W_\phi^{\mathrm{asym}}(x,y)$ are the rotationally asymmetric terms at ϕ rotational angle. Therefore, most rotationally asymmetric terms, except for the $kN\theta$ terms, are determined.

The rotationally symmetric terms and $kN\theta$ terms in the traditional shift-rotation method are reconstructed from the lateral shifting test [11]. However, a single shifting test indicates the insufficiency of difference equations to solve all the wavefront information. Therefore, the Zernike-based algorithm can only be employed to characterize the low-frequency surface figure [5]. In comparison, the lateral shearing method can determine the wavefront information of all CCD pixels through two or more shifting tests and the least squares fitting algorithm. However, the lateral shearing method cannot determine the astigmatism aberration accurately [9]. Therefore, the presented method in this section uses multiple rotational tests to determine astigmatism and most other rotationally asymmetric terms. It also adopts two orthogonal lateral shifting tests to reconstruct the rotationally symmetric and $kN\theta$ terms with pixel-level resolution.

At ϕ rotational angle, let $T_\phi^x(x,y)$ and $T_\phi^y(x,y)$ be the test results when the test optics are shifted in the X and Y directions, respectively. $T_\phi^x(x,y)$ and $T_\phi^y(x,y)$ are given as

$$T_\phi^x(x,y) = W_\phi(x-s_x,y) + V(x,y), \tag{6}$$

and

$$T_\phi^y(x,y) = W_\phi(x,y-s_y) + V(x,y), \tag{7}$$

where $W_\phi(x-s_x,y)$ is the surface figure with an s_x shift in the X direction and $W_\phi(x,y-s_y)$ is the surface figure with an s_y shift in the Y direction.

The system error will be cancelled by comparing Eqs. (2), (6), and (7). The following finite difference equations can be derived as

$$\begin{aligned}T_\phi(x,y)-T^x_\phi(x,y)&=W_\phi(x,y)-W_\phi(x-s_x,y)\\&=[T_\phi(x,y)-\bar{T}(x,y)]\\&\quad-[T_\phi(x-s_x,y)-\bar{T}(x-s_x,y)]\\&\quad+[W^{\mathrm{sym}}_\phi(x,y)+W^{kN\theta}_\phi(x,y)]\\&\quad-[W^{\mathrm{sym}}_\phi(x-s_x,y)+W^{kN\theta}_\phi(x-s_x,y)]\end{aligned} \quad (8)$$

and

$$\begin{aligned}T_\phi(x,y)-T^y_\phi(x,y)&=W_\phi(x,y)-W_\phi(x,y-s_y)\\&=[T_\phi(x,y)-\bar{T}(x,y)]\\&\quad-[T_\phi(x,y-s_y)-\bar{T}(x,y-s_y)]\\&\quad+[W^{\mathrm{sym}}_\phi(x,y)+W^{kN\theta}_\phi(x,y)]\\&\quad-[W^{\mathrm{sym}}_\phi(x,y-s_y)+W^{kN\theta}_\phi(x,y-s_y)].\end{aligned} \quad (9)$$

The rotationally symmetric terms $W^{\mathrm{sym}}_\phi(x,y)$ and $kN\theta$ terms $W^{kN\theta}_\phi(x,y)$ can be reconstructed by solving the difference between Eqs. (8) and (9).

The typical wavefront reconstruction algorithm with a pixel-level resolution is based on the least squares fitting, which is usually used in the lateral shearing method. However, such algorithm bears a large noise propagation ratio because it usually requires a small shift of one pixel to avoid a singular solution [3]. To reduce the noise propagation ratio and maintain pixel-level resolution, an algorithm applicable for large shifts is proposed as follows. The wavefront that results from the CCD sensor of the interferometer can be described by an $M \times M$ square matrix. The shift distances are P pixels in the X direction and Q pixels in the Y direction. The wavefront Ω involved in the difference equations will be separated into $P \times Q$ sub-apertures $\Omega_{p,q}(p = 1, 2, \ldots P; q = 1, 2, \ldots Q)$. Sub-aperture $\Omega_{p,q}$ is made up of columns $x = p, p + P, p + 2P, \ldots$ and rows $y = q, q + Q, q + 2Q, \ldots$ of the original wavefront. In this case, the shift distance is one pixel for every subaperture. Therefore, all unknown subwavefronts can be reconstructed using the standard least squares fitting algorithm. Finally, the original wavefront is obtained by combining all the known subwavefronts. Figure 1 shows how the wavefront is separated into six subapertures when the shift distances are three pixels in the X direction and two pixels in the Y direction.

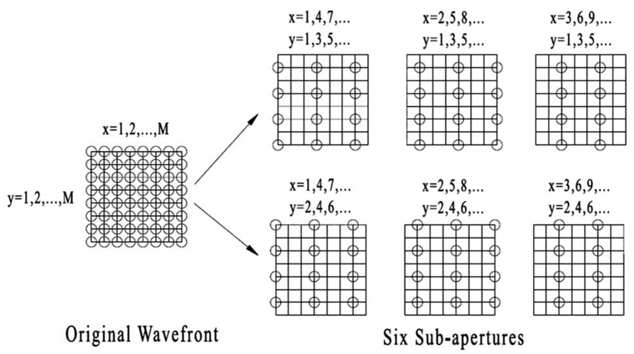

Fig. 1. Separating procedure of subapertures.

3. NUMERICAL SIMULATION AND ABSOLUTE TESTING EXPERIMENTS

Numerical simulation was performed to determine the characteristics of the extended shift-rotation method. Two actual wavefronts (1057 × 1057 pixels) in Fig. 2 were used as the system error and the surface figure. Figure 2(a) is an actual $\lambda/40$ PV transmission sphere reference surface with figure error of 2.97 nm RMS (system error); Fig. 2(b) is the surface figure error of a spherical surface in our laboratory with figure error of 2.45 nm RMS (surface figure of the test optics).

The two wavefronts could construct the testing results at N rotational positions and two lateral shifting positions by rotating and shifting the surface figure. The N rotational positions should be equispaced. Then, the wavefront reconstruction algorithm described above was applied to reconstruct the surface figure.

The main error sources of the shift-rotation method are reproducibility (statistic error) and the shift error during lateral shifting (systematic error) [13]. Therefore, increasing rotational positions to reconstruct the surface figure information as much as possible with rotational tests is preferable. Considering both the testing accuracy and efficiency, 12 rotational tests were selected for the numerical simulation. Figure 3 shows the wavefront reconstruction procedure and result in detail. The high-frequency rotational symmetric and $12k\theta$ terms of the surface figure were revealed. Therefore, the entire surface figure was determined with a pixel-level spatial resolution. The reconstructed surface figure (Fig. 3(k) is nearly identical to the surface figure provided in Fig. 2(b). The difference between the two figures is only 0.0013 nm RMS when the shift distance is 16 pixels.

Figure 4 shows the relation between the wavefront reconstruction error and the shift distance. When the reconstructed surface figure is subtracted from the given surface figure pixel to pixel, the RMS of the difference wavefront is defined as the wavefront reconstruction error. As shown by the blue dashed line, the wavefront reconstruction error without testing noise (algorithm error) is well within 0.01 nm RMS (relative error 0.4%) when the shift distance is less than 55 pixels. Assuming the shift error is one pixel, the red solid line shows that the wavefront reconstruction error (noise propagation ratio) could be reduced by 70% by increasing the shift distance from 8 to 55 pixels.

Figure 5 shows the relation between the execution time of the wavefront reconstruction procedure and the shift distance. The number of the subapertures that can be divided is related to the shift distance. As the shift distance increases, the subaperture number increases, and the pixel number of each

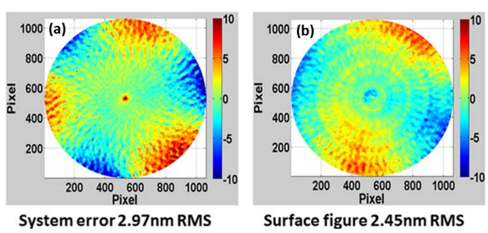

Fig. 2. Two wavefronts for numerical simulation: (a) is the system error and (b) is the surface figure of the test optics.

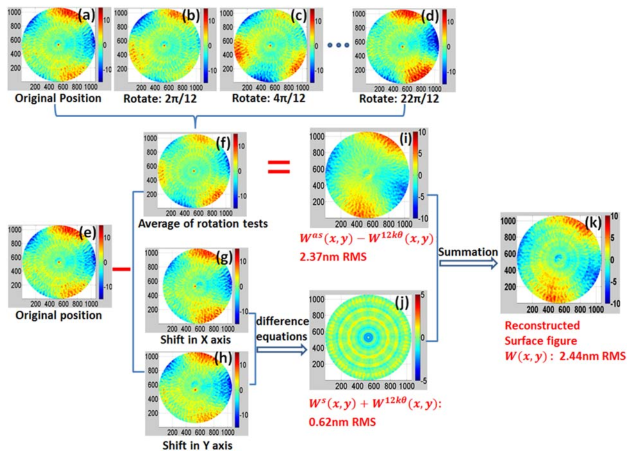

Fig. 3. Wavefront reconstruction procedure and result: (a) and (e) are the test results at the original position; (b), (c), (d) are the test results at other rotational positions, $T_\phi(x,y)$, $(\phi = 2\pi/N, 4\pi/N, \ldots, 2\pi/(N-1)/N)$; (f) is averaged result of all rotational positions, $\bar{T}(x,y)$; (g) and (h) are the test results in the X and Y directions, $T_\phi^x(x,y)$, $T_\phi^y(x,y)$, respectively; (i) is the reconstructed wavefront by all the rotational test results; (j) is the reconstructed wavefront by the shifted test results; (k) is the entire reconstructed wavefront.

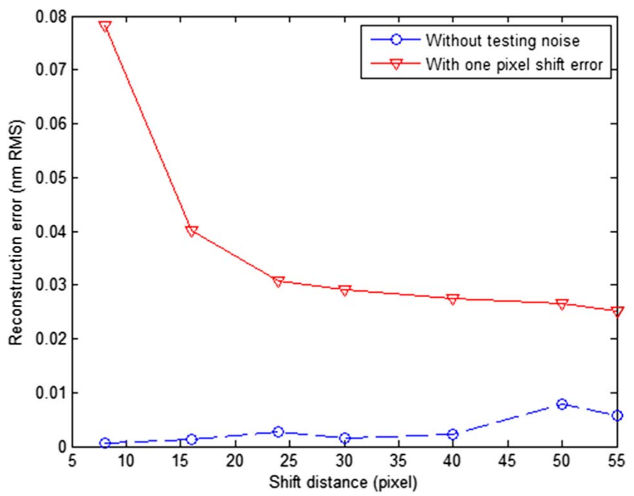

Fig. 4. Relation between wavefront reconstruction error and shift distance. The blue dashed line is the wavefront reconstruction error without testing noise. The red solid line is the wavefront reconstruction error with one pixel shift error.

subaperture is reduced, which makes the execution time shorter.

The system error and the figure error of the testing optics used in the execution time simulation in Fig. 5 are the two wavefronts (1057 × 1057 pixels) shown in Fig. 2. When the shift distance is 6, 8, 16, 32, 64, and 128 pixels in the X and Y directions, the entire wavefront can be divided into 36 (6 × 6), 64 (8 × 8), 256 (16 × 16), 1024 (32 × 32), 4096 (64 × 64), and 116384 (128 × 128) subapertures, respectively. The corresponding execution times are 290.9 min, 101.9 min, 12.9 min, 2.1 min, 0.8 min, and 0.6 min, as shown in Fig. 5 below. The computer we used is a Lenovo workstation, and the

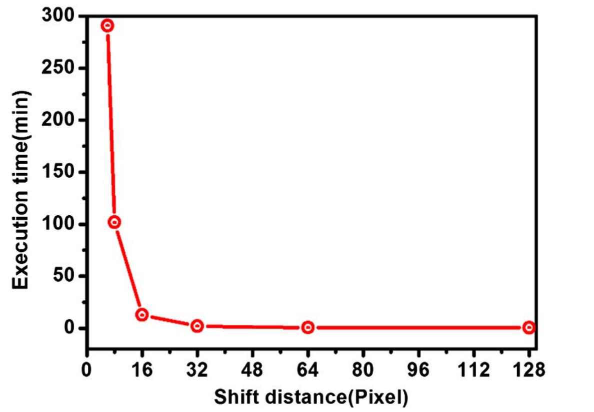

Fig. 5. Relation between the execution time of the wavefront reconstruction procedure and the shift distance.

specifications are as follows: (1) processor: Intel(R) Xeon(R) CPU E5-2630 v3 at 2.40 GHz (32 CPUs), ~2.4 GHz; 2) installed memory (RAM): 32 GB; 3) system type: 64-bit Windows 7 Professional Operating System.

However, as the shift distance increases, the shift error of the translation mechanism also increases. Considering the computational error, the computational efficiency, and the shift error of the actual shift mechanism, we generally chose a shift of 16–40 pixels in the experiments.

4. EXPERIMENTAL RESULTS AND CROSS-CHECK

Absolute testing experiments of spherical optics were carried out using the presented method. A Fizeau interferometer (Zygo, MST) was used to test a spherical surface based on the methods described above. The experimental setup is shown in Fig. 6. The angular position error of the rotational mechanism is $\pm 10''$. The shift position error of the shift mechanism is ± 15 μm. A vibration eliminator is used to suppress vibration of the granite stage, and the vibration is better than vibration criterion E (VC-E). The temperature of our laboratory is controlled. The temperature is kept at 22°C, and the fluctuating range of the temperature is less than ± 0.02°C. The spherical surface is of concave shape with a clear aperture (CA) of 90 mm and a radius of curvature of 340 mm. The pixel number of the

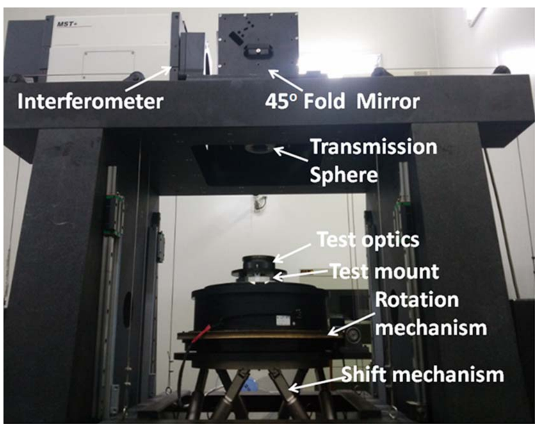

Fig. 6. Photo of the absolute testing setup.

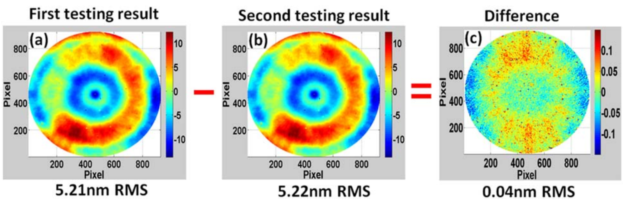

Fig. 7. Reproducibility of the absolute testing. (a) The first test result, (b) the second test result, (c) the wavefront difference between the two test results.

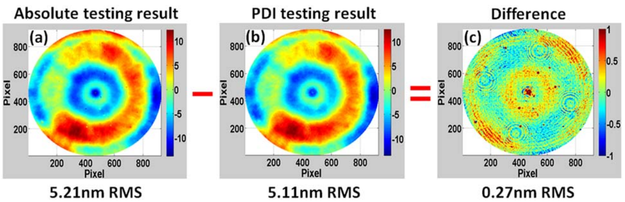

Fig. 8. Experimental results and crosscheck of absolute testing and PDI testing. (a) Test result with the presented absolute testing method, (b) test result with homemade PDI instrument, (c) the difference between the two methods.

CCD used in the interferometer is 1200 pixel × 1200 pixel. The test resolution is 0.97 mm/pix. The absolute testing procedure included 12 rotational tests and 2 shifting tests with shift distances of 32 pixels.

In the above-mentioned experimental conditions, the repeatability of testing the concave surface can reach 0.03 nm RMS. The reproducibility of the absolute testing can reach 0.04 nm RMS, as shown in the following Fig. 7. The repeatability is the wavefront difference of two successive test results without readjusting the test optics. The reproducibility is the wavefront difference of two test results of the test optics, but the test optics are removed from their test mount and readjusted for the second measurement.

The cross-check result is shown in Fig. 8. Figure 8(a) is the absolute testing result with the presented absolute testing method. The concave spherical surface was also measured with the method using a PDI and the testing result is shown in Fig. 8(b). The PDI setup was developed by us. The test resolution is 1.58 mm/pix when the PDI was used to test the above-mentioned concave spherical surface. Detailed information about the PDI setup can be found in Ref. [14]. The absolute test result based on the Fizeau interferometer is subtracted from the test result with PDI pixel to pixel; the wavefront difference of both measurements was 0.27 nm RMS, which is shown in Fig. 8(c). If we assume statistical independence of the interferometer errors, we obtain an error of 0.19 nm RMS for both interferometers accordingly. The experimental results prove that the extended shift-rotation method has potential subnanometer testing uncertainty with high spatial resolution.

5. CONCLUSION

In this paper, an extended shift-rotation method with large shifts is presented to obtain the surface figure of spherical surfaces absolutely with pixel-level spatial resolution and low noise propagation ratio. The presented method combines the advantages of the traditional shift-rotation and the lateral shearing methods. The testing procedure includes N equi-spaced rotational tests and two orthogonal lateral shifting tests. This method can also be used for the absolute testing of plane surfaces if the tilt of the test optics is controlled by other ways. Large shifts and the subaperture wavefront reconstruction algorithm are proposed to improve the noise propagation ratio and avoid a singular solution. The surface figure of all the spatial frequency domains can be revealed by this method. Algorithm error can be controlled well within 0.4%, and noise propagation ratio could be improved greatly by increasing the shift distances. In addition, the execution time of the wavefront reconstruction procedure is reduced because the wavefront was divided into multiple subapertures. The difference of the measurement results from the presented absolute testing method and the method using a PDI showed that the absolute testing uncertainty reached 0.19 nm RMS. The cross-check result indicated that the presented method has potential subnanometer testing uncertainty.

Funding. National Natural Science Foundation of China (NSFC) (21603211).

Acknowledgment. We thank the State Key Laboratory of Applied Optics for the use of their equipment.

REFERENCES

1. E. E. Bloemhof, "Absolute surface metrology by differencing spatially shifted maps from a phase-shifting interferometer," Opt. Lett. **35**, 2346–2348 (2010).
2. S. Okuda, T. Nomura, K. Kamiya, H. Miyashiro, K. Yoshizawa, and H. Tashiro, "High-precision analysis of a lateral shearing interferogram by use of the integration method and polynomials," Appl. Opt. **39**, 5179–5186 (2000).
3. G. Harbers, P. J. Kunst, and G. W. R. Leibbrandt, "Analysis of lateral shearing interferograms by use of Zernike polynomials," Appl. Opt. **35**, 6162–6172 (1996).
4. H. Ichikawa and T. Yamamoto, "Apparatus and method for wavefront absolute calibration and method of synthesizing wavefronts," U.S. patent 5,982,490 (9 November, 1999).
5. K. Otaki, T. Yamamoto, Y. Fukuda, K. Ota, I. Nishyama, and S. Okazaki, "Accuracy evaluation of the point diffraction interferometer for extreme ultraviolet lithography aspheric mirror," J. Vac. Sci. Technol. B **20**, 295–300 (2002).
6. D. Su, E. Miao, Y. Sui, and H. Yang, "Absolute surface figure testing by shift-rotation method using Zernike polynomials," Opt. Lett. **37**, 3198–3200 (2012).
7. B. Dörband and G. Seitz, "Interferometric testing of optical surfaces at its current limit," Optik **112**, 392–398 (2001).
8. D. Su, "Research on absolute testing of the optical surface figure," Ph. D. dissertation (University of Chinese Academy of Sciences, 2013).
9. C. J. Evans and W. P. Kuhn, "Method and apparatus for tilt corrected lateral shear in a lateral shear plus rotational shear absolute flat test," U.S. patent 7,446,883 (4 November, 2008).
10. D. Malacara, *Optical Shop Testing* (Wiley, 2007).
11. W. Song, F. Wu, X. Hou, and Y. Wan, "Optimized absolute testing method of shift-rotation," Appl. Opt. **52**, 7028–7032 (2013).
12. H. Glatzel, D. Ashworth, M. Bremer, R. Chin, K. Cummings, L. Girard, M. Goldstein, E. Gullikson, R. Hudyma, J. Kennon, B. Kestner, L. Marchetti, P. Naulleau, R. Soufli, and E. Spiller, "Projection optics for extreme ultraviolet lithography (EUVL) microfield exposure tools

(METs) with a numerical aperture of 0.5," Proc. SPIE **8679**, 867917 (2013).
13. F. Schillke, "Critical aspects of testing aspheres in interferometric setups," Proc. SPIE **3739**, 317–324 (1999).
14. J. Yu, H. T. Zhang, C. S. Jin, D. M. Ma, H. Wang, and Z. X. Lu, "Ultra-high accuracy point diffraction interferometer: development, accuracy evaluation and application," Proc. SPIE **9684**, 96840T (2016).